UC Davis

UC Davis Previously Published Works

Title

Quantum Simulations of Radiation Damage in a Molecular Polyethylene Analog.

Permalink

https://escholarship.org/uc/item/9pb944kk

Authors

Troup, Nathaniel

Kroonblawd, Matthew

Donadio, Davide

et al.

Publication Date

2024-10-22

DOI

10.1002/marc.202400669

Peer reviewed

eScholarship.org Powered by the California Digital Library
University of California

Macromolecular Rapid Communications
www.mrc-journal.de

Quantum Simulations of Radiation Damage in a Molecular Polyethylene Analog

Nathaniel Troup, Matthew P. Kroonblawd, Davide Donadio, and Nir Goldman**

An atomic-level understanding of radiation-induced damage in simple polymers like polyethylene is essential for determining how these chemical changes can alter the physical and mechanical properties of important technological materials such as plastics. Ensembles of quantum simulations of radiation damage in a polyethylene analog are performed using the Density Functional Tight Binding method to help bind its radiolysis and subsequent degradation as a function of radiation dose. Chemical degradation products are categorized with a graph theory approach, and occurrence rates of unsaturated carbon bond formation, crosslinking, cycle formation, chain scission reactions, and out-gassing products are computed. Statistical correlations between product pairs show significant correlations between chain scission reactions, unsaturated carbon bond formation, and out-gassing products, though these correlations decrease with increasing atom recoil energy. The results present relatively simple chemical descriptors as possible indications of network rearrangements in the middle range of excitation energies. Ultimately, the work provides a computational framework for determining the coupling between nonequilibrium chemistry in polymers and potential changes to macro-scale properties that can aid in the interpretation of future radiation damage experiments on plastic materials.

1. Introduction

Polyolefins (i.e., thermoplastics derived from alkenes) have wide-scale industrial and commercial use in lightweight plastic products due to their inexpensive starting materials as well as their ease of synthesis. Polyethylene, (PE; $[C_2H_4]_n$), in particular accounts for 36% of the total plastics market, with uses in packaging film, trash and grocery bags, wire and cable insulation, squeeze bottles, toys, and housewares.[1] Its mechanical properties can be controlled by changes in the polymer's structure, such as varying the hydrocarbon chain length, molecular weight distribution, degree of crosslinking (inter-chain bonding), and overall structure due to thermal annealing.[2–4] Ionizing radiation is an established environmental stressor that can have a large effect on polymers' physical and chemical properties. In this case, some form of high-energy radiation, e.g., gamma radiation, x-rays, or electron beam, is applied to the polymer and ultimately alters its structure through the creation of crosslinks, chain scissions, graft copolymerization, oxidation and/or compatibilization, and/or morphology stabilization.[2] This can have a drastic effect on material properties, allowing for great tunability for specific application needs, such as hardening for upcycling purposes (e.g., for use in building materials),[5] the manufacturing of nanogels for controlled drug delivery,[6] and creation of artificial muscles.[7] Ionizing radiation is known to degrade polymer insulated cables in nuclear power plants,[8] though it can be used as a reliable means of sterilization of medical devices[9,10] and food packaging,[11] as well as degradation of plastic packaging for recycling purposes.[2,12] However, the spectrum of energy absorption and loss as a function of radiation fluence is not fully characterized for many polymers,[13–15] and fundamental aspects of the material response to radiation remain poorly quantified.

Experimental radiation damage studies tend to rely on accelerated aging studies,[16,17] where samples are exposed to high dose rates (e.g., tens of kGy over days) as well as elevated temperatures. Highly empirical theories (e.g., constitutive models)[18] in turn are used to extrapolate experimental results out to actual service conditions (e.g., decades), where models are largely untested due to a dearth of experimental data. Physical and chemical effects in these cases are generally integrated responses, where ionization and heating occur simultaneously and over relatively short timescales.[19–21] This coupling poses difficulty in terms

N. Troup, N. Goldman
Department of Chemical Engineering
University of California Davis
One Shields Avenue, Davis, CA 95616, USA
E-mail: goldman14@llnl.gov
M. P. Kroonblawd, N. Goldman
Physical and Life Sciences Directorate
Lawrence Livermore National Laboratory
Livermore, CA 94550, USA
D. Donadio
Department of Chemistry
University of California Davis
One Shields Avenue, Davis, CA 95616, USA
E-mail: ddonadio@ucdavis.edu

The ORCID identification number(s) for the author(s) of this article can be found under https://doi.org/10.1002/marc.202400669

© 2024 The Author(s). Macromolecular Rapid Communications published by Wiley-VCH GmbH. This is an open access article under the terms of the Creative Commons Attribution-NonCommercial License, which permits use, distribution and reproduction in any medium, provided the original work is properly cited and is not used for commercial purposes.

DOI: 10.1002/marc.202400669

of unambiguously correlating radiation with specific changes in properties of interest, such as viscosity, gelation, stress-strain responses, or out-gassing products.[20,22–26] Hence, predictions of polymer-radiation interactions require a thorough understanding of the evolution of the polymer functional properties in the presence of environmental stressors. Elucidation of these effects would place confidence intervals on current aging studies and could accelerate material/upcycling design.

In this regard, quantum simulations are a powerful tool for understanding the chemical processes that occur within polymers by modeling local chemical changes as a function of radiation dose. Density Functional Tight Binding (DFTB) is a semi-empirical quantum method that holds promise as a simulation approach that can have comparable accuracy to higher-order methods (such as Kohn–Sham Density Functional Theory) while yielding substantial improvements in computational efficiency. Briefly, the DFTB total energy expression is derived directly from Kohn–Sham DFT assuming spherically symmetric charge distributions about neutral atoms and expanding the Kohn–Sham DFT Hamiltonian to the second or third order in charge fluctuations.[27,28] This yields the following total energy expression:

$$E_{\mathrm{DFTB}} = E_{\mathrm{BS}} + E_{\mathrm{Coul}} + E_{\mathrm{Rep}} \tag{1}$$

Here, E_{BS} corresponds to the band structure energy (from the approximate Kohn-Sham eigenstates) computed with a minimal basis set, and E_{Coul} is the Columbic term and accounts for charge transfer. E_{Rep} is the so-called "repulsive energy", which corresponds to ion-ion repulsions, as well as the Hartree and exchange-correlation double counting terms found in the DFT total energy expression. E_{Rep} generally is short-ranged and empirically fit, which allows for tuning the transferability and accuracy for specific applications as needed.[29–32] DFTB calculations scale as $\mathcal{O}\left(N^3\right)$ due to the solution for the approximate Kohn–Sham eigenvalues (similar to the underlying DFT method) which limits its accessible length scales. Regardless, the combination of approximate quantum mechanics and short-ranged empirical functions allows DFTB to retain most of the accuracy of Kohn–Sham DFT while achieving $10^2 - 10^3$ times improvement in computational efficiency.

In this work, we use amorphous decane (AD) as a model system for polyethylene in order to help shed light on the effects of radiation damage in a non-crystalline system, given that simulations of actual polymeric systems would require system sizes of thousands of atoms or greater,[13] which is cost-prohibitive with quantum simulation approaches. In addition, a decane molecule is a reasonable surrogate for modeling local chemistry given that its equilibrium end-to-end chain length (12.53 Å) is similar to the Kuhn length of PE (≈12 Å), i.e., the length at which polymer segments can be considered freely jointed or uncorrelated. We note that molecular dynamics (MD) simulations of radiation damage in polyethylene have been performed with an empirical reactive force field model,[14] though these simulations focused exclusively on crystalline polymers at low temperatures. We simulate the irradiation process through the Primary Knock-on Atom (PKA) method (e.g., ref. [33]), where a randomly selected atom is imparted with a recoil velocity over the range of 10 – 70 eV. We then categorize the resulting complex chemistry using our previously established graph theoretical approach.[34] Finally, we compute the conditional probabilities and statistical correlations between chemical events such as the out-gassing of small molecules with network rearrangement reactions. Ultimately, our work serves to place a bound on the possible damage modes due to PE radiolysis as well as the possible ramifications for mechanical and strength properties, which can help guide future simulation model development and experimental efforts.

2. Computational Methods

2.1. Generation of Initial Simulation Configurations

An initial decane molecule was created using the MOLTEMPLATE[35] tool. A condensed phase system was then established by periodically replicating the chain to form a low-density supercell of 0.01 g mL^{-1} with 11 decane molecules (352 atoms) in total. An initial disordered configuration was created by simulation at 600 K for 5 nanoseconds with a time step of 0.5 fs, using an Optimized Potential for Liquid Simulations (OPLS) force field,[36] with constant temperature (NVT) using Nosé–Hoover chain thermostats.[37] Subsequently, a two-stage equilibration process was utilized to reduce the temperature to 300 K and increase the density to 0.73 g mL^{-1}, similar to that of amorphous PE. The system temperature was first decreased to 400 K by using a temperature ramp for 5 ns, followed by an MD simulation at 400 K for an additional 5 ns. This was succeeded by constant pressure (NPT) simulation at 400 K and 1 atm for another 5 ns to increase the system's density using the Nosé–Hoover thermostat and barostat scheme.[38] Next, this sequence of NVT/NPT simulations was repeated, gradually lowering the system's temperature in 20 K increments of 1 ns until reaching our desired conditions. A concluding set of NPT simulations confirmed that the decane molecules had become non-diffusive. The resulting supercell had a cubic dimension of 15.32 Å. This allows for a large enough system to observe condensed-phase chemical reactivity while remaining tractable with quantum calculations. These simulations were performed using LAMMPS[39] (version 29-Oct2020).

The final frame from this simulation was then used to seed the subsequent DFTB simulations using the DFTB+ code (ver. 19.1).[40] For this work, we have used the pbc-0-3 parameter set,[41] though several exist that have sufficient accuracy for C-H-containing materials. The inclusion of spin-polarization[42,43] yielded no differences in product formations and hence was not used in our study. An initial NVT equilibration simulation was run for 5 ps at 300 K using a time step of 0.2 fs, with Fermi-Dirac smearing[44] of 300 K, SCC convergence of 10^{-6} au, and sampling of the Γ-point, only. Previous works showed that including spin-polarization has minor effects on the chemistry of alkane degradation, hence we do not consider it in our calculations.

2.2. Primary Knock-on Atom Simulations

Primary Knock-on Atom simulations were conducted with a similar procedure to previous efforts.[34,45] Here, a reaction cascade is induced by imparting a high-energy velocity with a random direction to a randomly selected carbon or hydrogen atom. These kinetic energies in general are taken to be significantly larger than

© 2024 The Author(s). Macromolecular Rapid Communications published by Wiley-VCH GmbH

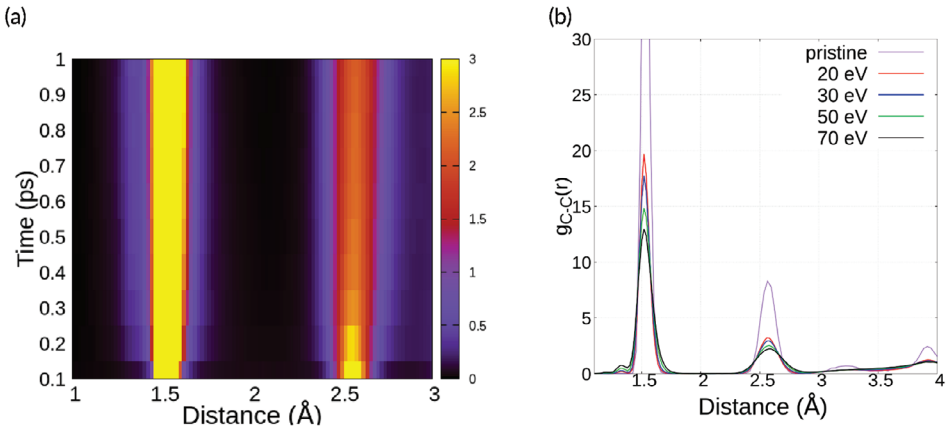

Figure 1. a) Heat map of the C–C radial distribution function (RDF) of a single 70 eV PKA simulation as a function of time. The backbone chemistry reaches a steady state within several hundred fs. b) C–C RDF plots for the non-irradiated system and for systems equilibrated after PKA excitations at different energies. Higher excitation energies result in a monotonic increase of unsaturated carbon bonds.

typical bond energies (e.g., tens of eV) which then induce rapid bond breaking in the system. In doing so, we can then place an upper bound on the expected radiation-induced degradation in our system.

The subsequent reaction cascades were sampled through ensembles of statistically independent constant energy (NVE) simulations that were 20 ps in length. Each PKA simulation included a short-timescale ballistic period on the order of one ps, followed by forming a chemical steady state at elevated temperature. Thermal relaxation is known to take tens of picoseconds or longer in soft organic materials subjected to sudden increases in temperature.[46] We have used a time step of 0.20 fs for the duration of the simulation. The electron Fermi–Dirac smearing temperature was set to 2000 K to account for the elevated ionic kinetic energy.

The ensembles of PKA simulations were created by assigning target recoil velocities separately to hydrogen or carbon with energies of 10, 20, 30, 50, or 70 eV. The 10 and 20 eV PKA sets consisted of 100 total simulations, while the remaining sets each consisted of 200 total simulations to better sample the more complex chemical pathways that ensued. The hydrogen PKA simulations tended to yield smaller amounts of chemical reactivity, possibly due to smaller ion size and lighter mass. In addition, carbon atoms have a higher absorption cross-section and thus are more likely to serve as an initial point for chemical degradation in PE experiments. Hence, our discussion for the remainder of the paper focuses on the carbon PKA simulations, only. This consists of a total of 800 statistically independent simulations across all PKA excitation energies, or 2 ns of total simulation time for the 10 and 20 eV events, and 4 ns total simulation time for 30, 50, and 70 eV events.

3. Results and Discussions

3.1. Initial Chemical Analysis and Nomenclature of Products

The C–C radial distribution functions (RDF) indicate that the PKA simulations achieve a chemical steady state within one picosecond of simulation time (**Figure 1**a). In the 70 eV case, double and triple bonds (1.3–1.4 Å) generally form within the first 300 fs after the PKA event and remain throughout the simulation. At this PKA energy, we observe a steady state temperature of 800 K after the excitation, leading to the thermal broadening of the RDF peaks with respect to ambient conditions. C–C RDFs for all excitation energies were calculated by averaging over the final 50 fs of each simulation and compared to the RDF of the system before PKA (Figure 1b). Our results show that increasing energy excitation leads to an increase in carbon double and triple bonds, and a concurrent decrease of the nearest-neighbor peak at ≈1.5 Å. Our results also indicate the presence of a diversity of carbon compounds at each PKA energy.

We have created a general picture of the carbon backbone reactivity by computing the probability of a chain scission or backbone-growing reaction occurring in our simulations as a function of PKA energy. Here, a simulation is counted as having either a scission or condensing reaction based on a single occurrence within that simulation. We use the well-established bonding criteria of the first minimum of the corresponding RDF (e.g., ref. [47]), yielding values of r_{CC} = 1.9 Å, r_{HH} = 1.1 Å, and r_{CH} = 1.5 Å. We note that there exists the possibility of a single simulation exhibiting both scission and growing reactions.

Overall, we observe a monotonic increase in chain scission and backbone growth as a function of increasing PKA energy (**Figure 2**). In particular, the 10 eV simulation set exhibited relatively little reactivity, with scission events occurring in only ≈3.0% of the simulations, and the remaining 97.0% exhibiting intact decane molecules without any growing reactions. In contrast, the 70 eV simulation set yielded a ≈76.8% chance of exhibiting scission reactions and 11.6% growing reactions, with the remaining 11.6% yielding no net reactivity. Backbone growing reactions were significantly less probable in all of our simulation sets, with the 20 eV set yielding a probability of 5.0%, the 30 eV set yielding a probability of 3.9%, and the 50 eV set yielding a probability of 11.1%, similar to the 70 eV set. The predominance of chain scission reactions in model polymeric systems like these is consistent with previous results for PKA simulations of soft materials.[34,45] Chain scission is a predominant radiolysis product in ultra-high molar mass polyethylene,[48] although PE can favor crosslinking overall.[2]

© 2024 The Author(s). Macromolecular Rapid Communications published by Wiley-VCH GmbH

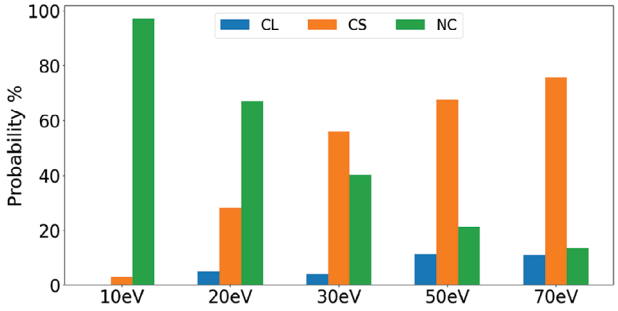

Figure 2. Distribution of chain reactions following excitation. The graph illustrates the probabilistic outcomes of an excited polymer chain, categorized into chain scission (CS), cross-linking (CL), and no change (NC), as a function of excitation energy (eV). For each excitation energy level, the sum of CS, CL, and NC probabilities totals 100%, representing the comprehensive breakdown of possible chain reactions.

Similar to our previous work, a graph theory analysis was used to distinguish between the broad range of unique chemical species with degenerate chemical formulae and bonding arrangements that can occur upon degradation.[34,45,49,50] Briefly, in our approach hydrogen atoms are first removed from the all-atom trajectory and covalent connectivity is assessed using our predefined bonding distance criteria. The open-source graph analysis software NetworkX[51] was then used to create an all-inclusive library of isomorphically distinct structures using the VF2 algorithm.[52] Backbone structures from our library were then flattened for easier visual inspection using a damped MD approach.[34] The library was then classified and analyzed in our statistical approaches.

Our isomorphic chemical library could be sorted into broad categories for various common degradation products (**Figure 3**, with abbreviations listed in **Table 1**). Our results suggest that a reactive event that increases the number of decane backbone atoms by a single carbon atom is relatively frequent. To better focus our analysis on the formation of larger products, we thus choose a chain length of 11 carbon atoms as the threshold between short and long carbon chains. Subsequently, we define "Y-links" (YL) species as those with a small carbon side-group (typically 1-2 carbon atoms) and where the longest carbon-chain segment ranges from three to 11 atoms. "Crosslinked" species (CL) refers to longer Y-linked chains where the longest segment contains 12 carbon atoms or more. Cyclic groups (CYCL) include both in-chain (backbiting) and free cyclic groups, such as methyl-

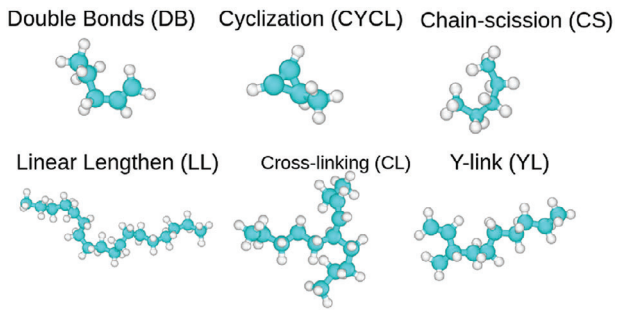

Figure 3. Categories of chemical products found in our PKA simulations, with carbon atoms colored in teal and hydrogen atoms in white.

Table 1. List of abbreviations for radiolysis product categories.

Feature	Abbreviation
Cross-linked	CL
Cyclization	CYCL
Y-links	YL
Longer linear chains	LL
Chain scission	CS
Hydrogen gas	H_2
methane/ethane	C-Gas
Unsaturated C–C bonds	DB

cyclopentane. The most frequent CYCL products involved three and four-member rings connected to a longer aliphatic chain. Longer linear chains (LL) correspond to linear carbon chains with more than 12 atoms. Chain scission (CS) refers to compounds with linear carbon backbones of length eight or less. Reaction products containing unsaturated carbon bonds (DB) largely consisted of double bonds with smaller amounts of C—C triple bonds. These were identified based on visualization of the molecules and the numbers of carbon and hydrogen atoms in the compound. It is important to note that individual molecules could exhibit multiple chemical features. For example, a large molecule might be classified as both CL and CYCL, depending on the final product.

Finally, the label "C-Gas" encompasses any carbon chain with a backbone length of two or fewer atoms, such as methane, ethane, ethene, and ethyne. Larger carbon gas molecules were generated at higher PKA excitations (i.e., propane and butane), albeit in trace amounts, and were classified as chain-scission or CS products. The designation "H_2" refers to molecular hydrogen formation within the system.

3.2. Chemical Statistics and Correlations

We now analyze the statistical properties of the radiolytic chemistry in terms of our predefined chemical groups. We first tally the total number of occurrences of each product type per simulation, with 95% confidence intervals determined via bootstrapping with 10 000 resamplings of each PKA ensemble (**Figure 4**). We find that most product types show a monotonic increase in the rate of occurrence as a function of PKA energy. This includes the formation of CYCL groups, DB groups, C-Gas species, and H_2 molecules. In general, chemical reactivity in our 10 eV ensemble is uncommon, with occurrence rates of 0.05 or less for all observed products. DB formation is the most common reaction product overall, exhibiting 0.62 occurrences per simulation in the 20 eV ensemble, and increasing to ≈2.60 in the 70 eV ensemble. CS production exhibits the second-highest occurrence rate, increasing from 0.30 at 20 eV to a little more than 1.70 at 70 eV. C-Gas exhibits a slightly higher occurrence rate at 20 eV relative to CS, though the rate at 70 eV is smaller, at a bit above 1.0. By comparison, the H_2 occurrence rate exhibits a larger upward gradient, with only a single occurrence in our 20 eV ensemble, which increases to ≈1.63 at 70 eV. Our observed production of H_2 gas is consistent with previous experimental results.[53]

 © 2024 The Author(s). Macromolecular Rapid Communications published by Wiley-VCH GmbH

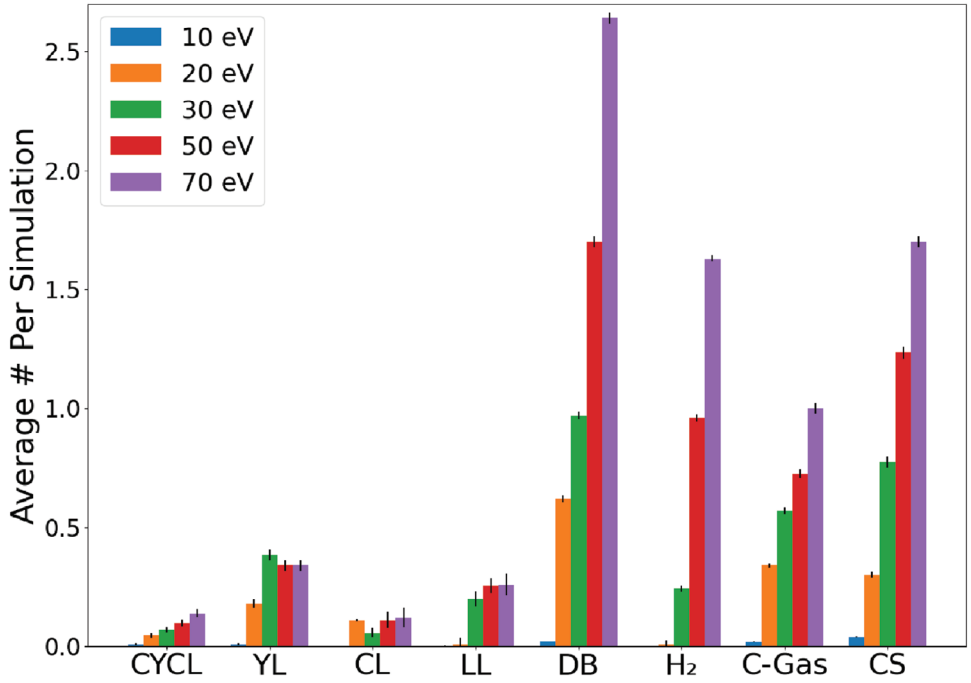

Figure 4. Histogram of the average rate of occurrence of each product class per simulation as a function of PKA energy. Error bars were calculated using the bootstrap method and represent a 95% confidence interval.

In contrast, the formation of CYCL species remains relatively rare for our entire simulation set, with the occurrence rate increasing to an average of approximately one out of five (0.2/simulation) in the 70 eV ensemble. CYCL groups were formed either through a single-chain backbiting mechanism, where the PKA-damaged chain folded over and bonded to itself or by a methyl ion reaction with a nearby decane chain to form a four-carbon ring within the middle of the backbone. We observe similarly low occurrence rates for YL, CL, and LL groups, with all four groups yielding values of less than 0.5 per simulation across the PKA energies in our study. The relatively high C-Gas production combined with the relatively low YL and CL production is consistent with the idea that PKA events in PE are conducive to chain scission reactions and less to cross-linking.[14]

We now analyze the conditional probabilities and their statistical correlation with a similar approach to our previous work.[45] Error bars correspond to the 95% confidence interval, as determined again by bootstrapping with 10 000 resamplings. We first define the unconditional probability $P(A)$ of a single reactive event A occurring in a PKA simulation of a given energy as:

$$P(A) = \frac{1}{N_{\text{sim}}} \sum E_A^{\text{sim}} \tag{2}$$

Here, E_A^{sim} is equal to a value of one if at least a single instance of a given product is detected in a simulation and zero otherwise, and N_{sim} is the number of simulations in that particular PKA set.

We can then define the joint unconditional probability $P(A \text{ and } B)$ for two events A and B as:

$$P(A \text{ and } B) = \frac{1}{N_{\text{sim}}} \sum E_{A+B}^{\text{sim}} \tag{3}$$

This corresponds to the probability that both A and B simultaneously have occurred in a simulation, without taking into account any notion of correlation or causation.

We can then use Equations (2) and (3) to compute the conditional probability $P(B|A)$ as follows:

$$P(B|A) = \frac{P(A \text{ and } B)}{P(A)} \tag{4}$$

In this case, $P(B|A)$ determines the probability that B occurs given that A has been detected in a simulation. The statistical correlation $\rho(A, B)$ between A and B can then be determined by the following equation:

$$\rho(A, B) = \frac{P(A \text{ and } B) - P(A)P(B)}{\sqrt{P(A)[1 - P(A)]P(B)[1 - P(B)]}} \tag{5}$$

Equation (5) yields values of $\rho(A, B)$ ranging from [− 1: 1], and is an indication of the degree of statistical coupling between two reactive events, or the extent to which two events are linearly related.

This analysis allows us to determine the strength of causality between chemical products. The conditional probability allows for a first pass in our chemical analysis, where we can determine which pairs of products have connected probabilities above a chosen threshold to warrant further investigation. This is es-

© 2024 The Author(s). Macromolecular Rapid Communications published by Wiley-VCH GmbH

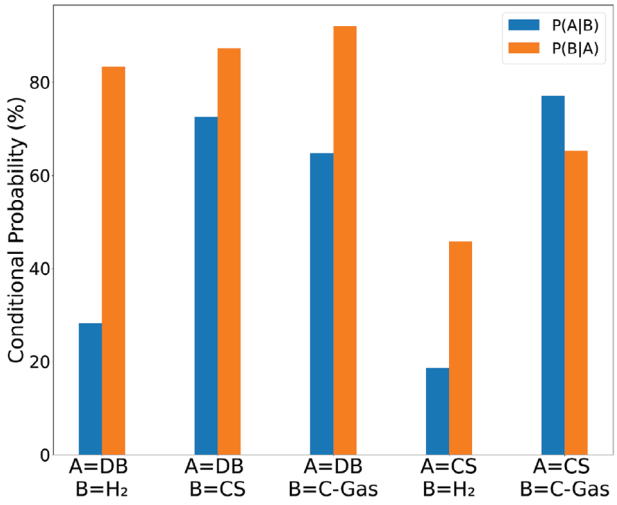

Figure 5. Highest conditional probabilities among the products of 30 eV PKA excitations. Pairs of products for which both $P(A|B)$ and $P(B|A)$ are high are shown.

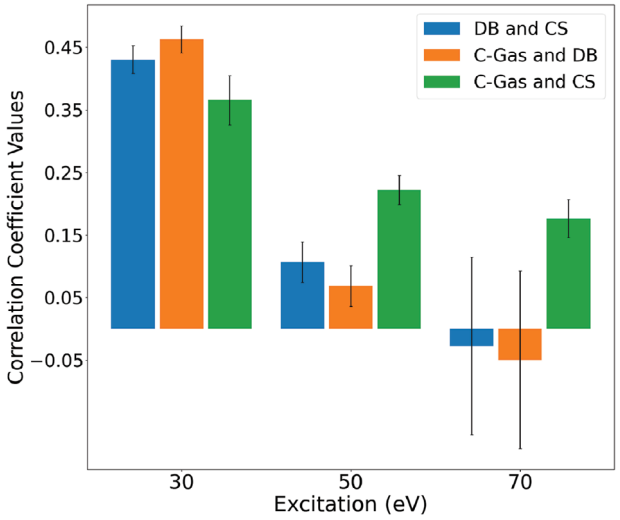

Figure 6. Correlation coefficients for 30, 50, and 70 eV simulation for a subset of product pairs with high conditional probabilities.

pecially useful in our study, given that our eight chemical categories yield 56 possible conditional probabilities, and that in general $P(B|A) \neq P(A|B)$. We can then use the correlation coefficient to determine the statistical link between product pairs. In doing so, we can help determine possible proxies for chemical events in polymer radiolysis that can be difficult to quantify, e.g., using carbon gas formation as an estimator for the degree of chain scissions.

We have computed full conditional probability matrices for all product pairs in all of our PKA simulation sets (Supporting Information), however, here we focus on a subset of the 30 eV excitation runs (**Figure 5**). The highest conditional probabilities observed in this case are between DB/H_2, DB/CS, DB/C-gas, CS/H_2, and CS/C-gas pairs. Several values of $P(B|A)$ (the probability of event B given the occurrence of event A) exceed 80%, where B corresponds to a DB group, and A corresponds to either H_2, C-Gas, or CS. We observe a value above 60% for B = CS and A = C-Gas, and a value close to 50% for B = CS and A = H_2. Several of these high values are chemically intuitive, as one would expect double bond formation to evolve hydrogen gas, and a chain scission reaction in our simulations would likely evolve carbon gas. The opposite values of $P(A|B)$ were smaller in most cases, due to the H_2 and C-Gas groups having higher numbers of formation pathways and consequently substantial correlations with several different chemical groups. Other conditional probabilities, such as P(DB|CS) and P(DB|C-gas) are less chemically intuitive and depend on the position of the excited carbon atom within the decane chain. For example, the excitation of a carbon atom in the middle of the chain can result in the formation of three fragments: a chain of length four (C4), one of length five (C5), and a CH_2 moiety. The C4 and C5 groups can often form double bonds, releasing hydrogen atoms that can eventually form H_2 molecules. Separately, the CH_2 group can react with hydrogen to form methane gas (CH_4).

Conditional probabilities from the 10 and 20 eV sets had substantially less product formation leading to large error bars. In contrast, results from the 50 and 70 eV sets exhibit larger values, though these are higher for all product pairs in our investigation. This is indicative of a higher degree of complexity between product correlations.

Given our identification of these five high-probability product pairs, we have computed their correlation coefficients for the 30, 50, and 70 eV simulation sets from Equation (5) (see Supporting Information for full results). Error bars are computed with bootstrap sampling, as before. The pairs from the 30 eV set that yielded the highest coefficient values are ρ(CS, H_2), ρ(CS, C-Gas), and ρ(CS, DB) (**Figure 6**). In all three cases, a potentially easier-to-measure result (H_2, C-Gas, DB) is coupled with a potentially harder-to-measure result (CS). We observe relatively strong correlations at 30 eV between all three pairs, with values of 0.43 for ρ(DB, CS), 0.46 for ρ(DB, C-Gas), and 0.36 for ρ(CS, C-Gas). We note that the ρ(DB, H_2) correlation is computed to be relatively low, with a value of 0.15. In this case, the joint probability of P(DB and H_2) is similar in magnitude to the product P(DB)P(H_2), yielding a small value in the numerator of Equation (5). This is indicative of the fact that while DB formation tends to yield H_2 synthesis, H_2 synthesis itself is produced from more than one reaction type and is a common product in all of our simulations. This is in contrast to our previous study regarding the creation of excited electronic states due to Møller scattering, where H_2 synthesis was a largely direct result of double bond formation, only.[50] Comparing and contrasting chemical products due to these different scattering processes is the subject of future work.

We observe that the higher energy PKA sets yield monotonically decreasing correlation coefficient values. For the 50 eV set, ρ(DB, CS) has decreased to 0.11, ρ(DB, C-Gas) to 0.07, and ρ(CS, C-Gas) to 0.22. These decrease further for the 70 eV set, with correlation coefficients of zero (within the 95% confidence interval) for ρ(DB, CS) and ρ(DB, C-Gas), and a value of 0.17 for CS/C-Gas. This trend is likely due in part to the higher degree of chemical reactivity and diversity of products at these elevated PKA energies. For example, the 30 eV yielded 100 simulations contain-

 © 2024 The Author(s). Macromolecular Rapid Communications published by Wiley-VCH GmbH

ing at least one DB event and 142 simulations with C-Gas. In contrast, the 70 eV set yielded 199 DB occurrences and 139 of carbon-gas. In addition, the 70 eV set yields higher occurrence rates of CYCL, YP, LL, and CL relative to the 30 eV set. The PKA energies explored in our work are high compared to the typical experimental scattering energies in polyethylene[50] and our results thus represent an upper limit in terms of what to expect from our statistical analysis.

4. Conclusion

In this work, we have used quantum Density Functional Tight Binding simulations to help quantify the degradation chemistry in polyethylene due to incident radiation. Our study has leveraged simulation cells consisting of disordered decane molecules held at a similar density to low-density polyethylene. Decane represents a sensible choice for our simulations given that its end-to-end length is very close to the persistent length commonly measured in polyethylene, while it is still small enough to be tractable with quantum simulation approaches. We then simulated the irradiation process through the Primary Knock-on Atom method, using excitation energies of 10, 20 30, 50, and 70 eV. The computational efficiency of our method allowed for 100–200 simulations per excitation energy, allowing for accurate statistical sampling of possible reaction pathways.

Our simulation results were then analyzed via a graph theory analysis toolkit to distinguish between different carbon backbone isomers and other structures as specifically as possible. Our results indicate that chain scission and H_2 out-gassing are amongst the most probable reactions, with significantly lower occurrences of backbones with higher carbon content. These results are in contrast to previous studies that observed that crosslinking could be more prevalent in systems with lower energy excitations such as those involving electronic excited states. We also observe the formation of double and triple carbon bonds, and methane and ethane out-gassing at excitations at 20 eV and above, with these species generally having the highest rates of occurrence in the 70 eV set.

We then used a statistical analysis to determine conditional probabilities and statistical correlation coefficients between different product groups for each set of PKA excitation energies. Our 30 eV simulation yields the richest results, where correlations between chain scission reactions and hydrogen and carbon gas production are relatively high. These results indicate the possibility of using the partial pressure of out-gassing species as a proxy measurement for the degree of change in chain scission in a polyethylene-containing system. Correlations between chain scission reactions and saturated carbon bond formation are also high within the 30 eV set due to a multi-step reaction mechanism, indicative of a second possible probe for chain scission reactions. These correlations are strongly diminished for the 50 and 70 eV sets, though, due to the increased chemical reactivity in those simulations as well as the larger degree of complexity of the chemical products.

Our work has focused on a "bottom-up" computational approach for understanding radiolysis and network rearrangements in polyethylene as a function of radiation dose. In particular, our quantum simulations and subsequent analysis can provide chemistry-based descriptors to help interpret polymer aging experiments, that can ultimately be used to create radiation-aware models for materials under a range of service or production conditions. Our calculations will have a significant impact on these types of studies, where the effects of heat and/or incident radiation on network rearrangements and subsequent changes in material strength and compressive properties are difficult to elucidate from experiments alone.

Supporting Information

Supporting Information is available from the Wiley Online Library or from the author.

Acknowledgements

This work was performed under the auspices of the U.S. Department of Energy by Lawrence Livermore National Laboratory under Contract DE-AC52-07NA27344.

Conflict of Interest

The authors declare no conflict of interest.

Data Availability Statement

The data that support the findings of this study are openly available in MaterialsCloud at DOI:10.24435/materialscloud:es-25, reference number 2024.156.

Keywords

molecular dynamics, polymer degradation, radiation damage

Received: August 19, 2024
Revised: October 10, 2024
Published online: October 22, 2024

[1] R. Geyer, J. R. Jambeck, K. L. Law, *Sci. Adv.* **2017**, *3*, e1700782.
[2] R. L. Clough, *Nucl. Instrum. Methods Phys. Res. Sect. B: Beam Interact. Mater. Atoms* **2001**, *185*, 8.
[3] V. Dakin, *Radiat. Phys. Chem.* **1995**, *45*, 715.
[4] J. Gehring, *Radiat. Phys. Chem.* **2000**, *57*, 361.
[5] A. V. Ponomarev, U. Gohs, C. T. Ratnam, C. Horak, *Radiat. Phys. Chem.* **2022**, *201*, 110397.
[6] Y. Yin, B. H. X. Yuan, L. Cai, H. Gao, Q. Yang, *Pharmaceutics* **2020**, *12*, 290.
[7] Q. M. Zhang, V. Bharti, X. Zhao, *Science* **1998**, *280*, 2101.
[8] A. Maléchaux, J. Colombani, S. Amat, S. R. A. Marque, N. Dupuy, *Polymers* **2021**, *13*, 1451.
[9] S. D. Bruck, E. P. Mueller, *J. Biomed. Mater. Res. Appl. Biomater.* **1988**, *22*, 133.
[10] I. R. Williams, M. B. Mayor, J. P. Collier, *Clin. Orthop. Relat. Res.* **1998**, *356*, 170.
[11] S. D. Chytiri, A. V. Badeka, K. A. Riganakos, M. G. Kontominas, *Food Addit. Contam.* **2010**, *27*, 546.
[12] L. González-López, L. Kearney, C. J. Janke, J. Wishart, N. Kanbargi, M. Al-Sheikhly, *Front. Chem.* **2022**, *9*, 803347.

 © 2024 The Author(s). Macromolecular Rapid Communications published by Wiley-VCH GmbH

[13] J. Polvi, P. Luukkonen, K. Nordlund, T. T. Järvi, T. W. Kemper, S. B. Sinnott, *J. Phys. Chem. B* **2012**, *116*, 13932.
[14] J. Polvi, K. Nordlund, *J. Appl. Phys.* **2014**, *115*, 023521.
[15] P. Stajanca, L. Mihai, D. Sporea, D. Negut, H. Sturm, M. Schukar, K. Krebber, *Opt. Mater.* **2016**, *58*, 226.
[16] F. Carrasco, P. Pagès, S. Pascual, X. Colom, *Eur. Polym. J.* **2001**, *37*, 1457.
[17] C. Maraveas, I. V. Kyrtopoulos, K. G. Arvanitis, T. Bartzanas, *Polymers* **2024**, *16*, 689.
[18] A. Maiti, R. H. Gee, T. Weisgraber, S. Chinn, R. S. Maxwell, *Polym. Degrad. Stab.* **2008**, *93*, 2226.
[19] S. Chinn, S. DeTeresa, A. Sawvel, A. Shields, B. Balazs, R. S. Maxwell, *Polym. Degrad. Stab.* **2006**, *91*, 555.
[20] A. Labouriau, C. Cady, J. Gill, D. Taylor, A. Zocco, J. Stull, K. Henderson, D. Wrobleski, *Polym. Degrad. Stab.* **2015**, *117*, 75.
[21] A. Labouriau, T. Robison, D. Geller, C. Cady, A. Pacheco, J. Stull, J. H. Dumont, *Polym. Degrad. Stab.* **2018**, *149*, 19.
[22] G. Camino, S. M. Lomakin, M. Lageard, *Polymer* **2002**, *43*, 2011.
[23] A. Charlesby, F. A. Freeth, *Proc. R Soc. Lond. A* **1955**, *230*, 120.
[24] A. A. Miller, *J. Am. Chem. Soc.* **1960**, *82*, 3519.
[25] E. Kornacka, J. Kozakiewicz, I. Legocka, J. Przybylski, G. Przybytniak, J. Sadło, *Polym. Degrad. Stab.* **2006**, *91*, 2182.
[26] J. A. LaVerne, N. A. I. Tratnik, A. Sasgen, *Radiat. Phys. Chem.* **2018**, *142*, 50.
[27] M. Gaus, Q. Cui, M. Elstner, *J. Chem. Theory Comput.* **2011**, *7*, 931.
[28] A. S. Christensen, T. Kubař, Q. Cui, M. Elstner, *Chem. Rev.* **2016**, *116*, 5301.
[29] V. Dantanarayana, T. Nemetiaram, D. Vong, J. E. Anthony, A. Troisi, K. N. Cong, N. Goldman, R. Faller, A. J. Moulé, *J. Chem. Theory Comput.* **2020**, *16*, 3494.
[30] N. Goldman, K. E. Kweon, B. Sadigh, T. W. Heo, R. K. Lindsey, C. H. Pham, L. E. Fried, B. Aradi, K. Holliday, J. R. Jeffries, B. C. Wood, *J. Chem. Theory Comput.* **2021**, *17*, 4435.
[31] M. Stöhr, L. Medrano Sandonas, A. Tkatchenko, *J. Phys. Chem. Lett.* **2020**, *11*, 6835.
[32] C. H. Pham, R. K. Lindsel, L. E. Fried, N. Goldman, *J. Phys. Chem. Lett.* **2022**, *13*, 2934.
[33] K. Nordlund, S. J. Zinkle, A. E. Sand, F. Granberg, R. S. Averback, R. E. Stoller, T. Suzudo, L. Malerba, F. Banhart, W. J. Weber, F. Willaime, S. L. Dudarev, D. Simeone, *J. Nucl. Mater.* **2018**, *512*, 450.
[34] M. P. Kroonblawd, N. Goldman, A. Maiti, J. P. Lewicki, *J. Chem. Theory Comput.* **2021**, *17*, 463.
[35] A. I. Jewett, D. Stelter, J. Lambert, S. M. Saladi, O. M. Roscioni, M. Ricci, L. Autin, M. Maritan, S. M. Bashusqeh, T. Keyes, R. T. Dame, J.-E. Shea, G. J. Jensen, D. S. Goodsell, *J. Mol. Biol.* **2021**, *433*, 166841.
[36] W. L. Jorgensen, J. Tirado-Rives, *J. Am. Chem. Soc.* **1988**, *110*, 1657.
[37] G. J. Martyna, M. L. Klein, M. Tuckerman, *J. Chem. Phys.* **1992**, *97*, 2635.
[38] G. J. Martyna, D. J. Tobias, M. L. Klein, *J. Chem. Phys.* **1994**, *101*, 4177.
[39] S. Plimpton, *J. Comp. Phys.* **1995**, *117*, 1.
[40] B. Hourahine, B. Aradi, V. Blum, F. Bonafé, A. Buccheri, C. Camacho, C. Cevallos, M. Y. Deshaye, T. Dumitrica, A. Dominguez, S. Ehlert, M. Elstner, T. van der Heide, J. Hermann, S. Irle, J. J. Kranz, C. Köhler, T. Kowalczyk, T. Kubar, I. S. Lee, V. Lutsker, R. J. Maurer, S. K. Min, I. Mitchell, C. Negre, T. A. Niehaus, A. M. N. Niklasson, A. J. Page, A. Pecchia, G. Penazzi, et al., *J. Chem. Phys.* **2020**, *152*, 124101.
[41] A. Sieck, T. Frauenheim, K. A. Jackson, *Phys. Status Solidi (B)* **2003**, *240*, 537.
[42] C. Köhler, G. Seifert, T. Frauenheim, *Chem. Phys.* **2005**, *309*, 23.
[43] C. Köhler, T. Frauenheim, B. Hourahine, G. Seifert, M. Sternberg, *J. Phys. Chem. A* **2007**, *111*, 5622.
[44] N. D. Mermin, *Phys. Rev.* **1965**, *137*, 1441.
[45] M. P. Kroonblawd, N. Goldman, A. Maiti, J. P. Lewicki, *Phys. Chem. Chem. Phys.* **2022**, *24*, 8142.
[46] M. P. Kroonblawd, B. W. Hamilton, A. Strachan, *J. Phys. Chem. C* **2021**, *125*, 20570.
[47] B. A. Steele, N. Goldman, I. F. W. Kuo, M. P. Kroonblawd, *Chem. Sci.* **2020**, *11*, 7760.
[48] A. L. Forster, Z. Tsinas, M. Al-Sheikhly, *Polymers* **2019**, *11*, 924.
[49] M. P. Kroonblawd, N. Goldman, J. P. Lewicki, *J. Phys. Chem. B* **2019**, *123*, 7926.
[50] M. P. Kroonblawd, A. Yoshimura, N. Goldman, A. Maiti, J. P. Lewicki, *J. Chem. Theory Comput.* **2022**, *18*, 5117.
[51] A. A. Hagberg, D. A. Schult, P. J. Swart, in *Proc. of the 7th Python in Science Conf.*, (Eds.: G. Varoquaux, T. Vaught, J. Millman), Los Alamos National Laboratory (LANL), Los Alamos, NM **2008**, pp. 11–15, Https://networkx.github.io (accessed May 15, 2024).
[52] L. P. Cordella, P. Foggia, C. Sansone, M. Vento, in *3rd IAPR-TC15 Workshop on Graph-based Representations in Pattern Recognition*, Cuen **2001**, pp. 149–159.
[53] G. Ungar, *J. Mater. Sci.* **1981**, *16*, 2635.
[54] L. Talirz, S. Kumbhar, E. Passaro, A. V. Yakutovich, V. Granata, F. Gargiulo, M. Borelli, M. Uhrin, S. P. Huber, S. Zoupanos, C. S. Adorf, C. W. Andersen, O. Schütt, C. A. Pignedoli, D. Passerone, J. VandeVondele, T. C. Schulthess, B. Smit, G. Pizzi, N. Marzari, *Sci. Data* **2020**, *7*, 299.

 © 2024 The Author(s). Macromolecular Rapid Communications published by Wiley-VCH GmbH